Bulletin of the Chemical Society of Japan

Self-assembly of Radially π-Extended Tetrathiafulvalene Tetramers for Visible and Near Infrared Electrochromic Nanofiber

Masashi Hasegawa* and Masahiko Iyoda*

Advance Publication on the web November 27, 2019
doi:10.1246/bcsj.20190283

Self-assembly of Radially π-Extended Tetrathiafulvalene Tetramers for Visible and Near Infrared Electrochromic Nanofiber

Masashi Hasegawa*[1] and Masahiko Iyoda*[2]

[1]Department of Chemistry, Graduate School of Science, Kitasato University, Sagamihara, Kanagawa 252-0373, Japan

[2]Department of Chemistry, Graduate School of Science, Tokyo Metropolitan University, Hachioji, Tokyo 192-0397, Japan

E-mail: masasi.h@kitasato-u.ac.jp

Masashi Hasegawa

Masashi Hasegawa received his Ph.D. from Tokyo Metropolitan University in 2004. He started his academic carrier as postdoctoral research in Tokyo Metropolitan University, Massachusetts Institute of Technology, and Ehime University. In 2007, he moved to Kitasato University as a research associate. His current research interests focus on creating novel π-conjugated compounds.

E-mail: iyoda@tmu.ac.jp

Masahiko Iyoda

Masahiko Iyoda received a Ph.D. degree (1974) in Chemistry from Osaka University. After postdoctoral work at Osaka University and the University of Cologne (with Prof. Emanuel Vogel), he returned to Osaka University in 1977 and became an Assistant Professor in 1978. In 1988, he became an Associate Professor in the Department of Chemistry, Osaka University. In 1991, he moved to Tokyo Metropolitan University (TMU) as a Full Professor. Since retirement from TMU in 2011, he has been working as a research professor at TMU. His research interests include the synthesis of functional π-electron systems and conjugated macrocycles, the noncovalent synthesis of functional supramolecular structures, and their applications in Materials Science.

Abstract

The self-assembly and electrochromic nanofiber formation of radially π-extended tetrathiafulvalene (TTF) tetramers anchored to 1,2,4,5-tetraethynylbenzene were investigated. The tetramer with SBu-substituents underwent self-assembly in solution. Cationic species of the tetramer, obtained by chemical oxidation with $Fe(ClO_4)_3$, exhibited a marked electrochromism in the solution. Their electronic spectra revealed absorption bands corresponding to intermolecular mixed-valence aggregation based on $(TTF//TTF)^{\bullet+}$, and π-aggregation based on $(TTF^{\bullet+}//TTF^{\bullet+})$ due to the strong molecular association in the cationic species. Furthermore, the tetramer formed an entangled nanoscale fibrous material from $CHCl_3$–hexane. Electrochemical oxidation of the nanofiber on an indium tin oxide electrode revealed a repeatable redox profile. The nanofiber displayed remarkable electrochromic behavior: the color of the fiber changed from purple (neutral) to brown/brownish green (dication and trication) and green (tetracation). These color changes of the nanofiber are similar to those in solution, and the electronic spectra of the oxidized nanofibers reflected the stacked TTF units in the cationic nanofibers.

Keywords: electrochromism, tetrathiafulvalene, nanofiber

1. Introduction

Apart from the initial research interest in electrical conductivity and superconductivity, tetrathiafulvalene (TTF) and its derivatives have been extensively utilized as building resources in the design of supramolecular chemistry and materials science.[1–10] TTF undergoes definite oxidation to give $TTF^{\bullet+}$ (radical cation) and TTF^{2+} (dication) at low oxidation potentials. These redox processes are repeatable, and hence TTF can be a trustworthy module for redox-triggered functional materials in host-guest chemistry,[11-14] positive electrode materials,[15,16] electrochromic (EC) devices,[17,18] and chiroptical switching materials.[19-24] Furthermore, the molecular self-assembly of TTF and its derivatives has become a superior vehicle leading to complex nanoscopic structures that are difficult to fabricate using electron beam lithography techniques as a top-down approach.[25-29] The strong intermolecular stacking by π–π and electrostatic force between $TTF^0//TTF^0$, $(TTF//TTF)^{\bullet+}$ (mixed-valence, MV), and $(TTF//TTF)^{2+}$ (π-dimer) can be expected both in solution and in solid state.[30-32] Thus, a variety of electroconducting one-dimensional (1D) nanofibers based on TTF derivatives have been developed through molecular self-assembly so far.[33-37]

When dealing with doped nanofibers (oxidized nanofibers), there are two pivotal stages that should be overcome. The first is the method for molecular assembly that can provide a long-range 1D ordering of cationic species in nanostructures. Highly adequate molecular design should be required for ordered nanofibers, because coulombic repulsion between cationic species prevents desirable molecular stacking.[38-40] The second is the doping method to generate unfilled open-shell electronic structures responsible for electrical conductivity. Exposure of neutral fibers to iodine vapor is commonly applied for the emergence of conductivity.[41-49] Nevertheless, the cationic state generated by adsorption of iodine vapor is usually unstable due to the easy desorption of iodine. Previously, we found that hexakis(tetrathiafulvalenylethynyl)benzene (**2a** in Figure 1) underwent strong molecular association in solution both in neutral and oxidized states.[50] The addition of excess amounts of

poor solvent (less polar solvent) into the solution containing self-assembled cationic species readily led to the electrical conducting nanofibers. However, such a successful example is still limited due to the fundamental difficulty in the formation of ordered structures consisting of cationic species. Therefore, our requirements of doped nanofibers forced us to develop alternate methods of preparing ordered cationic species.

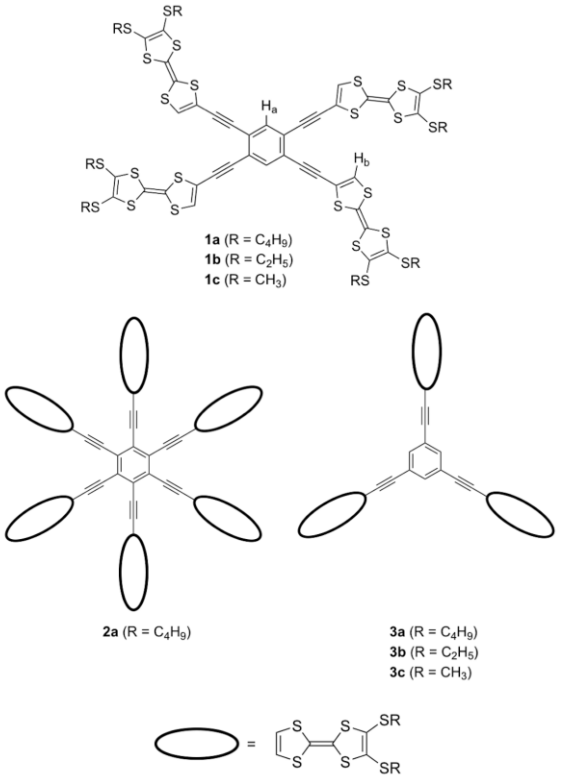

Figure 1. Chemical structures of radially π-extended tetrathiafulvalene oligomers (**1**–**3**)

Another possible approach is post-doping of the nanofibers by electric stimuli. The application of a proper voltage to the electrode where the nanofibers are deposited can easily lead to MV or higher oxidation states. Such electrochemical doping may be accompanied with multi-color EC behavior. Thus far, EC films based on electro-active organic or inorganic compounds have been developed because of their potential applicability in displays and smart electronics.[51-56] In 1979, Kaufman et al. achieved EC films based on polymer compounds having TTF moieties as a redox-active chromophore.[17] However, few studies have focused on EC materials composed of flexible nanofibers, gels, and other soft materials,[57–60] although they can be a promising component for wearable electronics in the future.

We have newly designed tetrakis(tetrathiafulvalenylethynylbenzene **1a** and **1b** for the core structure of self-assembled nanofibers. Although numerous TTF oligomers, extended with acetylene scaffolds such as **2a**, exhibit strong self-assembly leading to nanofibers,[61–67] they occasionally decompose under ambient conditions in solution owing to the intrinsic thermal instability of the acetylene scaffold. However, the previously reported **3a** and **3b** are stable despite weak self-assembly and no fiber formation.[68] Thus, the decrease in the number of ethynyl-TTF units from **2a** to that in the present system, could encourage both self-assembly and stability. We report herein, self-assembly and nanofiber formation that is stable enough to be treated under ambient conditions. In addition, facile formation of the MV nanofibers by electrical stimuli results in clear multi-step electrochromism and conventional regulation of the oxidation state in the nanofibers.

2. Results and Discussion

Synthesis. Synthesis of **1a** and **1b** was summarized in Scheme 1. Four TTF units were anchored by the Sonogashira coupling reaction of 1,2,4,5-tetraethynylbenzene, prepared from 1,2,4,5-tetrakis(trimethylsilylethynyl)benzene (**5**), with a iodo-TTF derivative (**6a** and **6b**). Compounds **1a** and **1b** were obtained as deep purple solids in moderate to good yields. The structures of **1a** and **1b** were fully characterized by ^{1}H and ^{13}C NMR, MS, IR, and UV-Vis spectra. Because of the extremely low solubility of octaethylthio derivative **1b**, further studies on the self-assembly and nanostructure formation were performed only on the octabutylthio derivative **1a**. Compound **1a** is much stabler than **2a** both in solution and solid state, and hence we can treat under ambient conditions without particular treatment. As a reference compound for **1a** and **1b**, 1,2-bis(tetrathiafulvalenylethynyl)benzene **4c** was prepared in 90% yield by a similar method.

Structural Analysis. Although single crystals of **1a** and **1b** suitable for X-ray analysis were not obtained, we have succeeded in X-ray structural determination of **4c** as a model for the half-unit of radially π-extended tetramer (Figure 2). Compound **4c** crystallizes in the monoclinic chiral space group $P2_1$. Compound **4c** has an almost planar structure except for the MeS-groups, and the two TTF units are aligned side by side with a tilting angle. One of two TTF units is slightly twisted toward the central benzene ring, while the other TTF unit and benzene ring are almost coplanar. There are two intramolecular S••H short contacts between the two TTF units: S(1)•••H(12) 2.811 Å and S(8)•••H(6) 2.994 Å, which are shorter than the sum (3.05 Å) of van deer Waals radii of sulfur (1.85 Å) and hydrogen (1.2 Å). Thence, the enantiomeric propeller-like structure in the crystal was induced by these interactions. Furthermore, **4c** stacks along the *b*-axis closely (Figure 2b) to form a one-dimensional columnar structure. The face-to-face distance between the S(1) atom and the neighboring least squares plane of TTF is found to be 3.62 Å. In addition, there are two additional S•••H interactions between stacked molecules.

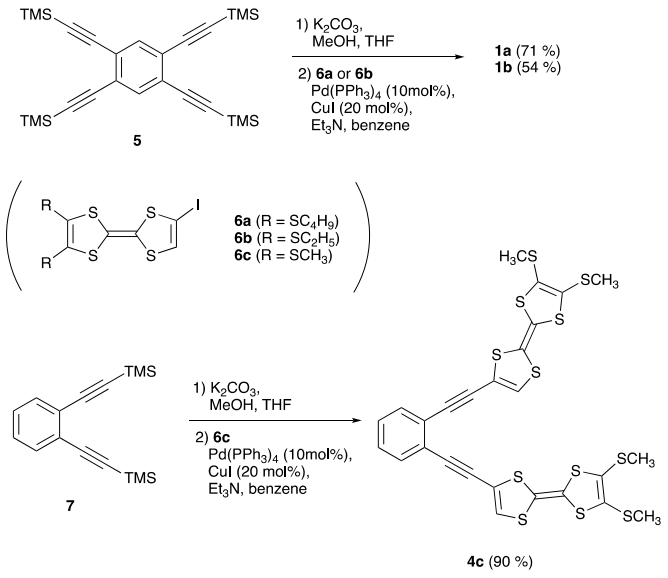

Scheme 1. Synthesis of **1a**, **1b**, and **4c**.

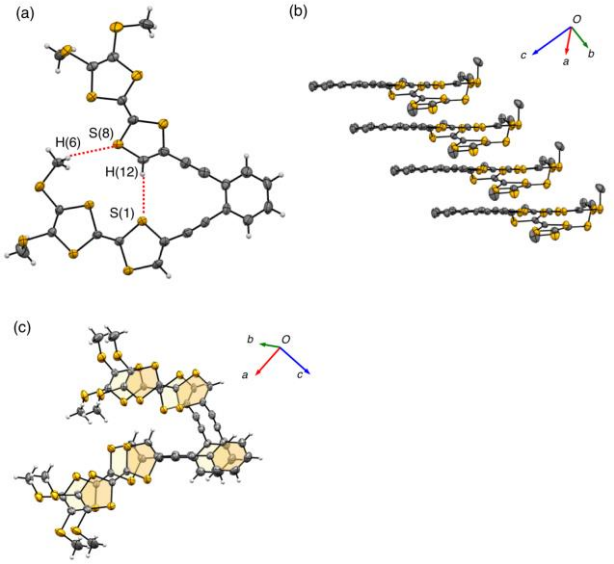

Figure 2. Synthesis of (a) ORTEP drawing of **4c**. Thermal ellipsoids are drawn at the 50% probability, (b) Crystal packing structure along the *b*-axis; hydrogen atoms are omitted for the sake of clarity, and (c) Stacking motif of **4c** (upper molecule: filled with orange and lower molecule: filled with light yellow).

A brief screening of geometry optimization of **1c** with SMe groups at B3LYP/6-31G(d,p) level of theory for several point groups suggested that both a conformation with D_2 symmetry (**1c**-i) and a propeller-like quasi-planar conformation with C_i symmetry (**1c**-ii) are relatively stable (Figure. 3). The former conformation has four TTF units anchored with an ethynylbenzene core in the parallel direction. However, the latter propeller-like conformation has two TTFs that tilt slightly from the central benzene ring so as to approximate a neighboring H atom (r = 3.12 Å in Figure. 3b). The dihedral angles ϕ_1 and ϕ_2 between the central benzene ring and TTFs are 19.7° and 3.91°, respectively. This conformation is similar to the molecular structure of **4c** found in the molecular packing in the crystal. Although the total energy of **1c**-ii (+0.9 kJ mol^{-1}) is slightly higher than that of **1c**-i in the gas phase, this conformation could be favorable for molecular packing in the solid state as found in the crystal structure of **4c**. The calculated HOMO and LUMO based on **4c**-ii geometry are illustrated in Figure 3c. The HOMO and almost degenerated HOMO–1 are mainly located on four TTF moieties, while the LUMO and almost degenerated LUMO+1 are located on the tetraethynylbenzene core. As for other conformations, essentially similar HOMO and LUMO descriptions were obtained. This is a typical tendency for extended TTF with an ethynyl–π scaffold.[50, 61–68]

The ^{1}H NMR spectrum of **1a** suggests an intramolecular S•••H contact in solution: chemical shift assigned to the H_b proton in **1a** (Figure. 1) was found at lower field of δ 6.74 ppm ($CDCl_3$, 20 °C) similar to the TTF proton of **4c** at δ 6.70 ppm ($CDCl_3$, 20 °C), while the corresponding protons of **6a** and **3a** were observed at δ 6.40 and 6.57 ppm, respectively. Such S•••H interactions could give a *pseudo*-planar geometry as a favored conformation despite the free rotation of the terminal TTF moieties.

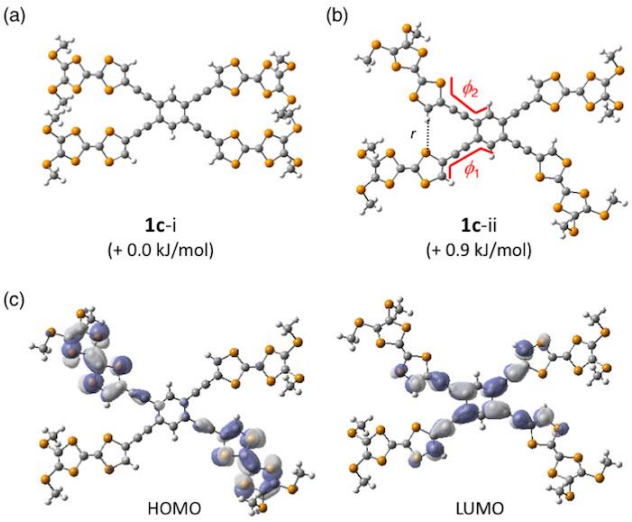

Figure 3. Calculated molecular structure of (a) **1c**-i and (b) **1c**-ii (r = 3.12 Å, ϕ_1 = 19.7°, ϕ_2 = 3.91°). (c) Frontier molecular orbitals of **1c**-ii calculated by B3LYP/6–31G(d,p).

Self-assembly in Solution. Radial tetramer **1a** displays self-assembly in solution, and their properties were studied by ^{1}H NMR spectra. The spectrum in $CDCl_3$ solution exhibited both concentration and temperature dependence. The signal assigned to the aromatic proton H_a of **1a** varied from δ 7.49 to 7.30 ppm as the concentration changed from 0.55 to 67.2 mM at 20 °C. In 15.9 mM solution, the chemical shift of H_a varied from δ 7.43 to 7.33 ppm as the temperature changed from 40 to –30 °C. This obvious upfield shift is due to the shielding effect of the benzene ring in the neighboring molecules when **1a** stacks in a face-to-face geometry. However, the TTF proton H_b did not show remarkable concentration dependence. Only small temperature dependence of a downfield shift less than 0.07 ppm was observed from 30 to –30 °C, presumably owing to the low shielding effect of the 1,3-dithiole ring associated with the intramolecular S•••H interactions.

Assuming a monomer-oligomer equilibrium (oligomeric association model) for the self-assembly of **1a**, the association constant (K_a) was determined to be 21.5 ± 3.1 M^{-1} at 293 K in $CDCl_3$.[69] Furthermore, thermodynamic parameters were also estimated from the results of variable temperature ^{1}H NMR experiments: ΔH = –16.7 (kJmol^{-1}) and ΔS = –31.3 (JK^{-1}mol^{-1}). The self-assembly appears to be driven by enthalpy, but opposed by entropy. The negative enthalpy value is due to the π-π stacking, van der Waals interactions, and S•••H interactions in the molecular stacking.

Redox Properties. The electrochemical properties of **1a** and **4c** were investigated by cyclic voltammetry (CV), and the redox potentials are summarized in Table 1 together with those of the related trimer **3a**.[68] As shown in Figure. 4a, the CV profile of **1a** in dilute solution (c = 1.0 x 10^{-5} M) displayed a broad reversible response centered at $E^1_{1/2}$ = 0.04 V and $E^2_{1/2}$ = 0.40 V (vs. Fc/Fc$^+$). The first anodic peak was found to be broad. Because the CV profile of **4c** exhibited similar redox waves at comparable potentials, the CV profile of **1a** revealed few intermolecular or intramolecular interactions between the TTF units through the acetylene scaffold (–ethynylene–phenylene–ethynylene–).[61] Hence, the two oxidation peaks in Figure. 4a correspond to the formation of **1a**$^{4+}$ and **1a**$^{8+}$, respectively. On the contrary, CV under concentrated conditions (c = 1.2 x 10^{-3} M) resulted in three pairs of well-dissolved reversible redox waves at $E^1_{1/2}$ = –0.06,

$E^2_{1/2}$ = 0.09, and $E^3_{1/2}$ = 0.40 V (V vs. Fc/Fc$^+$). Judging from the peak current ratio and molecular structure, the first and second oxidations can be attributed to the oxidation to **1a**$^{2+}$ and **1a**$^{4+}$ formation, respectively. The highest oxidation wave should correspond to the formation of **1a**$^{8+}$. As the intramolecular electronic interactions among the TTF moieties are negligible in this scaffold, [61] the formation of **1a**$^{2+}$, before the oxidation to **1a**$^{4+}$ implies intermolecular MV stacking based on (TTF//TTF)$^{\bullet+}$ or its larger aggregates.[70] Thus, the MV species (**1a**$^{2+}$)$_2$ were predominantly formed at E^1 in the concentrated conditions, following which the aggregates may undergo further oxidation at E^2. Such a redox profile was found in a series of TTFs in the radial oligomers of **2a**[50] , **3a**[68] and also found in trimeric or tetrameric stacking TTF system.[31]

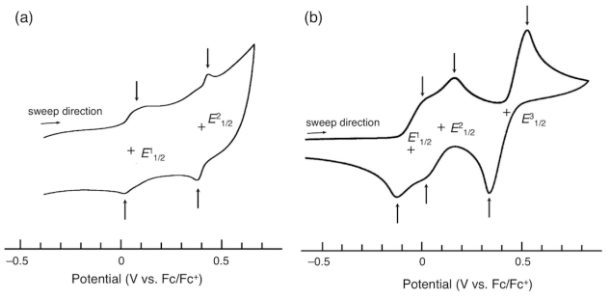

Figure 4. CV charts of **1a** in CH_2Cl_2 at 23 °C. (a) **1a**: 1.0 x 10^{-5} M and (b) **1a**: 1.2 x 10^{-3} M. Conditions: CH_2Cl_2, 0.1 M Bu_4ClO_4, all potentials were measured against an Ag/Ag$^+$ reference electrode and converted to vs. Fc/Fc$^+$.

Table 1. Redox potentials of **1a**, **4c**, and **3a** (V vs. Fc/Fc$^+$)

	Conc. (mM)	$E^1_{1/2}$ (V)	$E^2_{1/2}$ (V)	$E^3_{1/2}$ (V)
1a [a]	0.01	0.04 (4e$^-$)	0.04 (4e$^-$)	–
1a [a]	1.2	−0.06 (2e$^-$)	0.09 (2e$^-$)	0.40 (4e$^-$)
4c [a]	0.42	0.06 (1e$^-$)	0.37 (1e$^-$)	
3a [b]	5.4	−0.04 (3e$^-$)	−0.14 (3e$^-$)	−0.47 (6e$^-$)

[a] Measured in CH_2Cl_2. [b] Measured in PhCN (ref. 68).

Electronic Spectra of Cationic Species. We performed the chemical oxidation of **1a** with Fe(ClO$_4$)$_3$ in CH_2Cl_2-MeCN (v/v = 4:1) to afford cationic species. The addition of 1, 2, 3, 4, and 10 (excess) equivalents of Fe(ClO$_4$)$_3$ formed **1a**$^{\bullet+}$, **1a**$^{2+}$, **1a**$^{3+}$, **1a**$^{4+}$ and **1a**$^{8+}$, respectively (Figure 5). During the chemical oxidation, **1a** displayed clear electrochromism shown in Figure 5a.

The electronic spectrum of **1a** exhibits two absorption maxima at 514 and 320 nm (Table 2). These are typical absorption bands found in an acetylene-extended TTF framework.[48,50,61,68] The absorption band at 514 nm is associated with charge transfer electronic transition from the HOMO of the TTFs to the LUMO of the acetylene moieties, while the absorption at 320 nm involves the electronic transition within the TTF frameworks. The time-dependent (TD) DFT study of model compound **1c** at CAM-B3LYP/6-31G(d,p) level reproduced these transitions qualitatively (Figure S3).

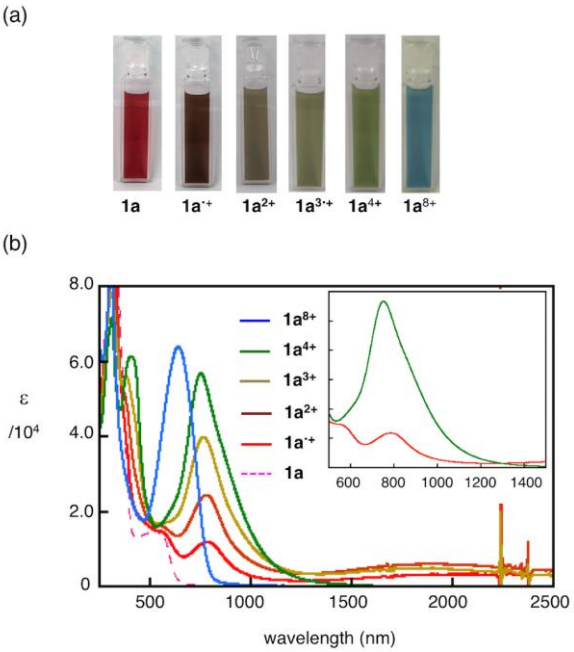

Figure 5. (a) Colors and (b) electronic spectra of **1a** (2.1 x 10^{-5} M), **1a**$^{\bullet+}$ (2.8 x 10^{-5} M), **1a**$^{2+}$ (2.8 x 10^{-5} M), **1a**$^{3+}$ (4.2 x 10^{-5} M), **1a**$^{4+}$ (3.4 x 10^{-5} M) and **1a**$^{8+}$ (1.5 x 10^{-5} M) in CH_2Cl_2-MeCN (v/v = 4:1) solution. The inset shows enlarged spectra of **1a**$^{\bullet+}$ and **1a**$^{4+}$.

Radical cation **1a**$^{\bullet+}$ exhibited very broad absorption at approximately 1800-2600 nm together with a prominent absorption at 783 nm (Figure 5b). This spectral feature is quite similar to that of the cationic species derived from **2a**[50] and **3a**,[68] which exhibit strong self-association in solution. The broad absorption can be attributed to the charge resonance (CR) in an MV state based on a (TTF//TTF)$^{\bullet+}$ stacking unit. On the contrary, the electronic spectra of radical cation **1c**$^{\bullet+}$ did not exhibit such a broad absorption in long wavelength region (Figure S9). On the basis of previous investigations of face-to-face arranged TTFs,[30,31] the two remarkable absorption bands are interpreted as a combination of stacked TTF units in an MV aggregate (Figure. 6a). They are assigned to the electronic transition from the HOMO to the SOMO (S_1, CR nature) and from the HOMO–1 to the SOMO (S_2) in stacked species of **1a**$^{\bullet+}$. These spectral outlines did not change even in dilute solution, indicating large association constants for the aggregation of dications and trications in solution.

Table 2. Absorption maxima of **1a** and its cationic species in CH_2Cl_2-MeCN (*v/v* = 4:1) solution [a]

	Color	Conc. (μM)	λ_{max} (nm)
1a	purple	21	320 (S_2), 514 (S_1)
1a$^{\bullet+}$	dark-brown	28	321, 550, [b] 783 (S_2), *ca.* 2060 (S_1)
1a^{2+}	brown	28	314, 550,[b] 778 (S_2), *ca.* 1900 (S_1)
1a^{3+}	brownish green	42	311, 385, 767 (S_2), *ca.* 1800 (S_1)
1a^{4+}	green	34	400, 750 (S_2), *ca.* 900 [b] (S_1)
1a^{8+}	blue	15	307, 640

[a] Spectra were measured in CH_2Cl_2-MeCN (v/v = 4:1). S_1 and S_2 denote electronic transitions described in Figure 6.
[b] Shoulder absorption.

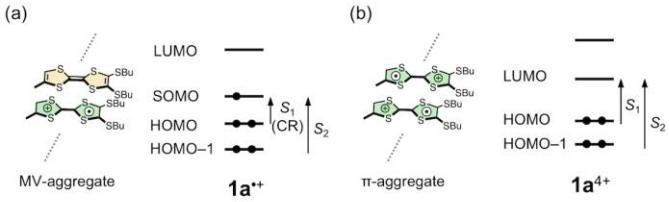

Figure 6. Possible electronic transitions of (a) MV-aggregate $(TTF//TTF)^{\bullet+}$ in $\mathbf{1a}^{\bullet+}$ and $\mathbf{1a}^{2+}$, and (b) π-aggregate $(TTF//TTF)^{2+}$ in $\mathbf{1a}^{4+}$.

In contrast, $\mathbf{1a}^{4+}$ exhibited no CR band in the NIR region. The electronic spectra exhibited absorption maxima at 750 and 400 nm. The former band tails with a shoulder peak (approximately 900 nm) up to 1400 nm are shown (Figure 5b, inset). The absorption maximum at 752 nm was blue-shifted compared to the S_2 band in $\mathbf{1a}^{\bullet+}$ (783 nm). This hypsochromic shift can be associated with the Davydov blue-shift because of the face-to-face stacking of $TTF^{\bullet+}$ in π-dimer or larger π-aggregates.[30-32] The broad shoulder is related to the HOMO-LUMO transition, which is essentially forbidden in a π-aggregate of $TTF^{\bullet+}$ (Figure 6b). As these experiments were performed under dilute conditions, $\mathbf{1a}^{4+}$ was stacked strongly in solution. Finally, the spectrum of $\mathbf{1a}^{8+}$ exhibited only a sharp absorption band at 640 nm, suggesting no association behavior of $\mathbf{1a}^{8+}$ due to the repulsion between the TTF^{2+} units.

On the other hand, the electronic spectra of the radical cations of $\mathbf{4c}^{n+}$ (n = 1, 2, and 4), which were prepared via oxidation using $Fe(ClO_4)_3$ under similar conditions, exhibited spectra based only on the oxidation of the TTF scaffold (Figure. S9). Therefore, there are neither intramolecular nor intermolecular interactions in the cations derived from **4c** in solution.

Nanofiber Formation. Compound **1a** formed a fibrous structure in $CHCl_3$-hexane solution. When hexane was added to a self-assembled solution of **1a** in $CHCl_3$, dark purple fibrous material appeared from the resultant cloudy suspension after several hours. Similar fibrous material was obtained by an ordinal reprecipitation procedure using $CHCl_3$ or CH_2Cl_2 with a poor solvent such as MeOH, EtOH, ether, or pentane. Scanning electron microscopy (SEM) measurements revealed that the fibril material from $CHCl_3$-hexane is composed of a slender and frizzled fiber structures (Figure 7a). The fibrils are approximately 100–200 nm thick and the length was above 20 nm. There is almost no concentration or solvent dependence of the morphology.

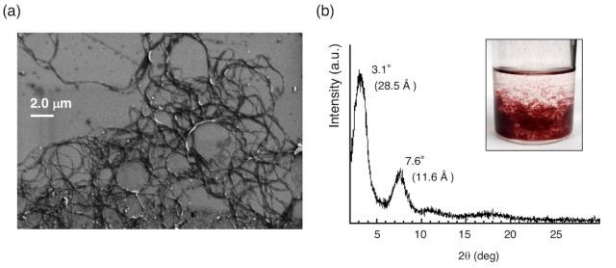

Figure 7. Scanning electron micrograph of the nanofibers of **1a** on an Si-wafer. (b) XRD profile of the nanofibers of **1a**. Inset shows appearance of the fibril material obtained from cloudy suspensions.

The longest absorption maximum of π-π* transition of **1a** fiber exhibited a red-shift reaching 530 nm (Table 3). The observed bathochromic shift compared to the absorption maximum of **1c** in $CHCl_3$ solution (514 nm) is attributed to the *J*-type aggregation (off-set geometry), which can be a similar arrangement found in the X-ray crystal packing of **4c**. The out-of plane X-ray powder diffraction (XRD) of as-cast **1a** fibers on the Al plate displayed a mostly amorphous halo with relatively weak peaks at 2θ = 3.10, 7.58° (*d* = approximately 28.5 and 11.6 Å) and some other ambiguous peaks (Figure. 7b). The observed *d*-spacing of the smallest 2 θ is comparable to the molecular size estimated from PM3-optimization of **1a** (35 Å) (Figure. S11). Therefore, compound **1a** was slip-stacked with face-to-face stacking to give a one-dimensional nanofiber. The addition of poor solvents may promote effective phase separation of aggregated **1a**.

Doping of the nanofibers, which are formed as a pellet shape, with I_2 vapor resulted in an inky-black nanofiber without collapse. The bulk electrical conductivities of the resultant fibers reached moderately high conductivities of σ_{rt} = 5.5 x 10^{-4} Scm^{-1}, reflecting the molecular stacking in the fiber structure (Figure. S12).

Electrochromic Properties of Nanofiber. The nanofibers of **1a** are thin enough, as observed in SEM measurements (Figure 7a), and hence we envisage that the nanofibers undergo oxidation by post-electrical doping on the electrode surface. We first measured redox properties of the nanofibers on an indium tin oxide (ITO) electrode (Figure 8a). The electrode, where the nanofibers were deposited, was immersed in MeOH containing 0.1 M Bu_4NClO_4 as the electrolyte. CV profiles between –0.4 and 0.8 V (vs. Fc/Fc^+) gave only irreversible anodic peaks (Figure S13), and nanofibers completely dissolved in MeOH beyond the second oxidation (> 0.2 V). However, repeatable redox cycles were observed without dissolution during the scanning of a narrower potential range (–0.4-0.18 V).

CV profiles were strongly affected by the scan rate. When faster scan rate of 100 mV/s was applied, a couple of semi-reversible peaks with wider peak-to-peak separation are recorded without remarkable color changes (Figure S15). In the fast-scanning condition, electron transfer might occur only on the surface, and hence the nanofiber could not undergo complete oxidation. On the contrary, when slow scanning of 1 mV/s was applied, several intense peaks were found (Figure 8a). In the oxidation process, a weak current response at approximately –0.15 V and an intense peak at 0.13 V were observed. In the cathodic scan, on the contrary, there are two peaks at 0.02 and –0.1 V. These redox profiles were repeatable without particular decomposition at least 10 times.

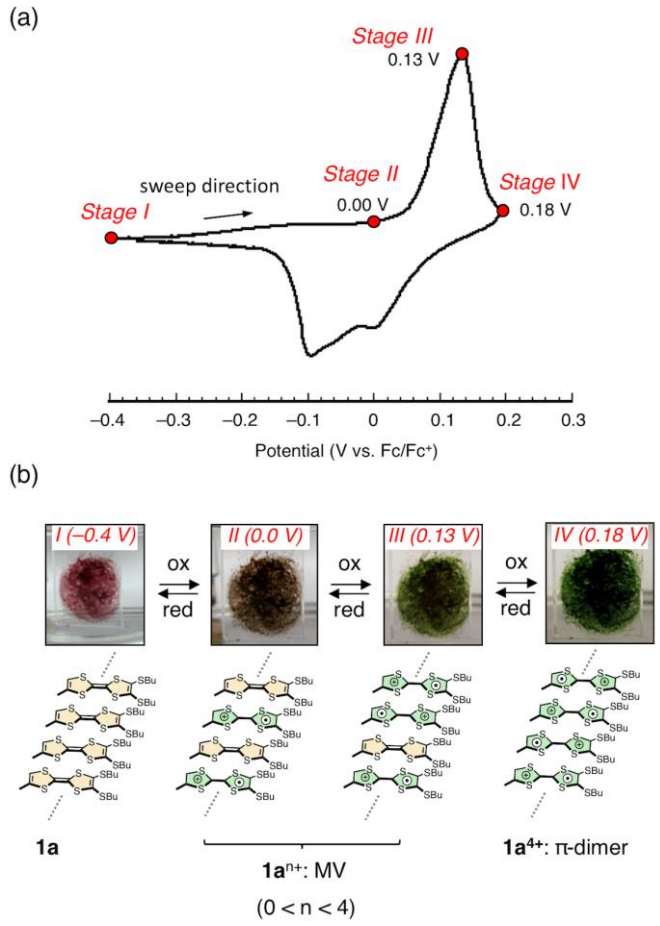

Figure 8. (a) Cyclic voltammograms of the nanofiber of **1a** with potential scan at 1 mV/s. (b) Photographs of the fibers of **1a** at I (–0.4 V), II (0.0 V), III (0.13 V) and IV (0.18 V) in the CV profile.

By comparison with the redox potentials of **1a** in solution, we can conclude that the first broad current response and the latter intense peak in the oxidation process can be attributed to the sequential formation of MV cationic species of $\mathbf{1a}^{n+}$ (n = 1, 2, and 3) and tetracation $\mathbf{1a}^{4+}$ in the nanofibers, respectively. In the range below 0.00 V, oxidation of **1a** to $\mathbf{1a}^{\bullet+}$ first occurs on the ITO electrode. Thereby, the injected hole can be quickly delocalized though π-π stacking in the nanofiber, although the diffusion of the anion into the fiber might be slow to lead to a weak current response. Then, the fiber continuously undergoes oxidation with the low anodic current until **1a** is oxidized to form $\mathbf{1a}^{3+}$ (< ca. 0.00 V). After that, oxidation corresponding to $\mathbf{1a}^{3+}/\mathbf{1a}^{4+}$ occurs with larger peak current. Similar oxidation profile was found in highly self-assembled species of **2a** in solution[50] and in π-conjugated polymer thin film deposited on the electrode.[71,72] However, in the reduction process, the first step at 0.02 can be assigned to the process from $\mathbf{1a}^{4+}$ to $\mathbf{1a}^{3+}$, correlating with the corresponding peak at 0.13 V in the oxidation process. The second peak at –0.1 V may correspond to the process from $\mathbf{1a}^{3+}$ to $\mathbf{1a}^{n+}$ (n = 2, 1, and 0), in which the reduction of $\mathbf{1a}^{3+}$ to $\mathbf{1a}^{2+}$ is the most energetically favorable process, exhibiting an intense peak. Such a large difference between the oxidation and reduction profile is presumably due to the difference of the rate in electrical doping/dedoping in the nanofibers on the electrode surface.

Table 3. Absorption maxima of self-assembled nanofibers of **1a** and its cationic species at various oxidation stages obtained by post-doping [a]

Ox. Stage [b] (Potential)	Conc. (mM)	color	λ_{max}
I (–0.40 V)	**1a**	Purple	530 (S_1)
II (0.00 V)	$\mathbf{1a}^{n+}$ (0 < n < 4)	Brownish green	550,[c] 818 (S_2), *ca.*1800 (S_1, *CR*) [c]
III (0.18 V)	$\mathbf{1a}^{4+}$	Green	418, 750 (S_2), *ca.* 1010 (S_1) [c]

[a] Spectra of the nanofibers were measured on an ITO electrode, which was immersed in MeOH containing Bu_4NClO_4 as the electrolyte. [b] Each oxidation stage was depicted in Figure 8a.
[c] Shoulder absorption.

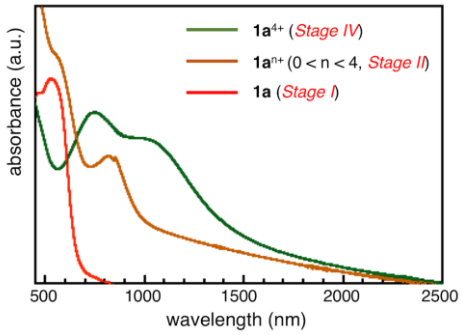

Figure 9. Electronic spectra of neutral and cationic nanofibers on quartz plate (**1a**) or ITO electrode ($\mathbf{1a}^{n+}$ and $\mathbf{1a}^{4+}$).

As shown in Figure 8b, the nanofiber on the electrode exhibited various colours. For instance, the colour gradually changes from purple to brown around 0.0 V (Stage II, in Figure 8a), brownish green around 0.13 V (Stage III, in Figure 8a), and then vivid green around 0.18 V (Stage IV, in Figure 8a) along the oxidation process. Opposite colour change — from green, brownish green, brown, to purple — was observed along the reduction process (Figure S16). These colour changes are almost coincident with those of cationic species in solution (Figure 5a). When the voltage is kept constant, the colour is also stationary without remarkable decomposition.[73] Thus, the electronic spectra can be collected at the selected stage (Table 3 and Figure 9). The electronic spectra at the constant voltage of 0.00 V on the anodic scan (Stage II, in Figure 8a) possess absorption maxima at 818 nm, together with a weak shoulder (Table 3). The former absorption band, assigned to the S_2 transition, exhibited a remarkable bathochromic shift compared to that of $\mathbf{1a}^{n+}$ (0 < n < 4) in solution (767–787 nm, Table 2). It is presumably due to the molecular stacking within the *J*-type arrangement that was solidified as the nanofiber in the neutral state before doping. The broad shoulder absorption (S_1), featured by CR nature in the stacked TTF units, was slightly weakened compared with that in solution. An off-set stacking based on molecular assembly in neutral solution may result in the decrement of this absorption band. When the constant voltage of 0.18 V (Stage IV in Figure 8) was applied, the green nanofiber exhibited characteristic absorption bands at 750 (S_2), together with shoulder absorption (S_1, λ_{max} = *ca*. 1010 nm) tails to 2500 nm. This spectrum curvature is quite similar to that of

typical dimeric TTFs in π-dimer form found in the literature.[30,31] While the S_2 band (750 nm) was found at a similar wavelength to that in solution of **1a**$^{4+}$ (S_2, 752 nm), a bathochromic shift and clear enhancement were observed in S_1 transition as compared to that in solution (approximately 900 nm), presumably due to its tight aggregation in the solid state.

4. Conclusion

We have synthesized TTF tetramers (**1a** and **1b**) anchored to a 1,2,4,5-tetraethynylbenzene scaffold. DFT calculations of **1c** and X-ray crystallographic analysis of **4c** revealed a stable molecular structure having intramolecular S••H interactions between two neighboring TTF moieties. ^{1}H NMR experiments of **1a** at various temperatures and concentrations in $CDCl_3$ suggest molecular self-assembly in solution, and the association constant (K_a) was determined (21.5 ± 2.0 M^{-1} at 20 °C). CV of **1a** in CH_2Cl_2 displayed two two-electron and one four-electron reversible redox responses in concentrated solution, although two four-electron redox waves were observed in dilute conditions. These differences are indicative of the intermolecular interactions between radical cations; furthermore, electronic spectra of radical cations, prepared by the chemical oxidation with $Fe(ClO_4)_3$, revealed their electronic structures. The oxidized species of **1a**$^{n+}$ ($0 < n < 4$) exhibited the intrinsic absorption of TTF$^{\bullet+}$ (S_2) and characteristic CR bands (S_1) in the NIR/IR region (1200-2500 nm), attributed to MV states among the intermolecular TTF stacks. Moreover, **1a**$^{4+}$ exhibited blue-shifted maximum absorption because of face-to-face stacked TTF$^{\bullet+}$ units in solution. One-dimensional nanofibers of **1a** were prepared from $CHCl_3$-hexane solution. The redox and electronic properties of the nanofibers were investigated using CV technique on an ITO electrode. Repeatable color changes were observed between **1a** (purple), **1a**$^{n+}$ ($0 < n < 4$) (brown and brownish green), and **1a**$^{4+}$ (green), and each color is associated with their oxidation stage. While the color of the nanofibers of **1a** at each oxidation stage is almost similar to that in solution, the electronic spectra of the fibers are affected by the molecular packing in the nanofibers. Although an approach to stationary doped-nanofibers without continuous electrical injection is still developing, our approach using the electrochemical oxidation of nanofibers on ITO electrode shows a new application of post-doping nanofibers.

Acknowledgement

We thank Prof. Dr. Kenro Hashimoto (The Open University of Japan), Mr. Jun-ichi Takano (Tokyo Metropolitan University), Dr. Kota Daigoku (Kitasato University), Dr. Yoshiyuki Kuwatani (VSN Inc.), and Prof. Dr. Yasuhiro Mazaki (Kitasato University) for the helpful discussion. This work was partially supported by the JSPS KAKENHI grants JP04J04136, JP16K17871, and JP18K05092. All calculations were performed at the Research Center for Computational Science, Okazaki (Japan).

Supporting Information

Instrumentation and materials, experimental procedures, NMR spectra, crystal data, cyclic voltammograms, and DFT studies. This material is available on http://dx.doi.org/10.1246/bcsj.

References

1. M. Hasegawa, M. Iyoda, Tetrathiafulvalene: A redox unit for functional materials and a building block for supramolecular self-assembly, in Organic Redox Systems: Synthesis, Properties, and Applications, (Ed.: T. Nishinaga), Wiley, 2015, pp. 89-125.
2. TTF Chemistry: Fundamental and Applications of Tetrathiafulvalene, (Eds.: J. Yamada, T. Sugimoto), Kodansha-Springer, Tokyo, 2004.
3. A. Jana, S. Bähring, M. Ishida, S. Goeb, D. Canevet, M. Sallé, J. O. Jeppesen, J. L. Sessler, *Chem. Soc. Rev.* **2018**, *47*, 5614.
4. V. Croué, S. Goeb, M. Sallé, *Chem. Commun.* **2015**, *51*, 7275.
5. F. Pop, N. Avarvari, *Chem. Commun.* **2016**, *52*, 7906.
6. S. Bähring, H. D. Root, J. L. Sessler, J. O. Jeppesen, *Org. Biomol. Chem.* **2019**, *17*, 2594.
7. D. Canevet, M. Sallé, G. Zhang, D. Zhu, *Chem. Commun*. **2009**, 2245.
8. V. A. Azov, *Tetrahedron Lett.* **2016**, *57*, 5416.
9. M. Iyoda, M. Hasegawa, Y. Miyake, *Chem. Rev*. **2004**, *104*, 5085.
10. J. L. Segura, N. Martín, *Angew*. *Chem. Int. Ed*. **2001**, *40*, 1372.
11. G. Barin, A. Coskun, M. M. G. Fouda, J. F. Stoddart, *ChemPlusChem*, **2012**, *77*, 159.
12. H. V. Scröder, H. Hupatz, A. J. Achazi, S. Sobottka, B. Sarkar, B. Paulus, C. A. Schalley, *Chem. Eur. J.* **2017**, *23*, 2960.
13. V. Croué, S. Goeb, G. Szalóki, M. Allain, M. Sallé, *Angew. Chem. Int. Ed.* **2015**, *55*, 1746.
14. J. S. Park, C. Bejger, K. R. Larsen, K. A. Nielsen, A. Jana, V. M. Lynch, J. O. Jeppesen, F. Kim, J. L. Sessler, *Chem. Sci.* **2012**, *3*, 2685.
15. M. Kato, K. Senoo, M. Yao, Y. Misaki, *J. Mater. Chem*. *A* **2014**, *2*, 6747.
16. J. Sun, Y. Wu, Y. Wang, Z. Liu, C. Cheng, K. J. Hartlieb, M. R. Wasielewski, J. F. Stoddart, *J. Am. Chem. Soc.* **2015**, *137*, 13484.
17. F. B. Kaufman, A. H. Schroeder, E. M. Engler, S. R. Kramer, J. Q. Chambers, *J. Am. Chem. Soc.* **1980**, *102*, 483.
18. C. Wang, A. S. Batsanov, M. R. Bryce, *Chem. Commun.* **2004**, 578.
19. M. Hasegawa, S. Iwata, H. Matsuzawa, Y. Mazaki, *Org. Lett.* **2011**, *13*, 4688.
20. K. Kobayakawa, M. Hasegawa, H. Sasaki, J. Endo, H. Matsuzawa, K. Sako, J. Yoshida, Y. Mazaki, *Chem. Asian J*. **2014**, *9*, 2751.
21. M. Hasegawa, J. Endo, S. Iwata, T. Shimasaki, Y. Mazaki, *Beilstein J. Org. Chem*. **2015**, *11*, 972.
22. M. Hasegawa, D. Kurebayashi, H. Matsuzawa, Y. Mazaki, *Chem. Lett.* **2018**, *47*, 989.
23. T. Biet, A. Fihey, T. Cauchy, N. Vanthuyne, C. Roussel, J. Crassous, N. Avarvari, *Chem. Eur. J.* **2013**, *19*, 13160.
24. E. Gomar-Nadal, J. Veciana, C. Rovira, D. B. Amabilino, *Adv. Mater*. **2005**, *17*, 2095.
25. M. Hasegawa, M. Iyoda, *Chem. Soc. Rev.* **2010**, *39*, 2420.
26. D. B. Amabilino, J. Puigmartí-Luis, *Soft Matter*. **2010**, *6*, 1605.
27. M. Iyoda, M. Hasegawa, *Beilstein J. Org. Chem*. **2015**, *11*, 1596.
28. M. Iyoda, M. Hasegawa, H. Enozawa, *Chem. Lett.* **2007**, *36***,** 1402.
29. S. S. Babu, S. Prasanthkumar, A. Ajayaghosh, *Angew. Chem. Int. Ed.* **2012**, *51*, 1766.
30. M. Hasegawa, K. Daigoku, K. Hashimoto, H. Nishikawa, M. Iyoda, *Bull. Chem. Soc. Jpn*. **2012**, *85*, 5.
31. M. Hasegawa, K. Nakamura, S. Tokunaga, Y. Baba, R. Shiba, T. Shirahata, Y. Mazaki, Y. Misaki, *Chem. Eur. J.* **2016**, *22*, 10090.
32. D.-W. Zhang, J. Tian, L. Chen, L. Zhang, Z.-T. Li, *Chem.*

Asian J. **2015**, *10*, 56.
33. R. Inoue, M. Hasegawa, Y. Mazaki, *Chem. Lett.* **2015**, *44*, 448.
34. F. Pop, C. Melan, I. Danila, M. Linares, D. Beljonnem D. B. Amabilino, N. Avarvari, *Chem. Eur. J.* **2014**, *20*, 17443.
35. H. Enozawa, M. Hasegawa, E. Isomura, T. Nishinaga, T. Kato, M. Yamato, T. Kimura, M. Iyoda, *ChemPhysChem* **2009**, *10*, 2607.
36. H. Enozawa, Y. Honna, M. Iyoda, *Chem. Lett.* **2007**, *36*, 1434.
37. M. Jørgensen, K. Bechgaard, T. Bjøernholm, P. Sommer-Larsen, L. G. Hansen, K. Schaumburg, *J. Org. Chem*. **1994**, *59*, 5877.
38. S. Ahn, Y. Kim, S. Beak, S. Ishimoto, H. Enozawa, E. Isomura, M. Hasegawa, M. Iyoda, Y. Park, *J. Mater. Chem*. **2010**, *20*, 10817.
39. C. Wang, D. Zhang, D. Zhu, *J. Am. Chem. Soc.* **2005**, *127*, 16372.
40. T. Akutagawa, K. Kakiuchi, T. Hasegawa, S. Noro, T. Nakamura, H. Hasegawa, S. Mashiko, J. Becher, *Angew. Chem., Int. Ed.* **2005**, *44*, 7283.
41. T. L. Gall, C. Pearson, M. R. Bryce, M. C. Petty, H. Dahlgaard, J. Becher, *Eur. J. Org. Chem.* **2003**, 3562.
42. J. Puigmartí-Luis, V. Laukhin, Á. P. del Pino, J. Vidal-Gancedo, C. Rovira, E. Laukhina, D. B. Amabilino, *Angew. Chem. Int. Ed.* **2006**, *46*, 238.
43. J. Puigmartí-Luis, Á. P. del Pino, E. Laukhina, J. Esquena, V. Laukhin, C. Rovira, J. Vidal-Gancedo, A. G. Kanaras, R. J. Nichols, M. Brust, D. B. Amabilino, *Angew. Chem. Int. Ed*. **2008**, *47*, 1861.
44. T. Kitamura, S. Nakaso, N. Mizoshita, Y. Tochigi, T. Shimomura, M. Moriyama, K. Ito, T. Kato, *J. Am. Chem. Soc.* **2005**, *127*, 14769.
45. T. Kitahara, M. Shirakawa, S. Kawano, U. Beginn, N. Fujita, S. Shinkai, *J. Am. Chem. Soc.* **2005**, *127*, 14980.
46. Sly, P. Kasák, E. Gomer-Nadal, C. Rovira, L. Górriz, P. Thordarson, D. B. Amabilino, A. E. Rowan, R. J. M. Nolte, *Chem. Commun.* **2005**, 1255.
47. Y. Kobayashi, M. Hasegawa, H. Enozawa, M. Iyoda, *Chem. Lett*. **2007**, *36*, 720.
48. H. Enozawa, T. Takahashi, T. Nishinaga, T. Kato, M. Hasegawa, M. Iyoda, *Bull. Chem. Soc. Jpn*. **2012**, *85*, 1120.
49. E. Isomura, T. Nishinaga, M. Iyoda, *Supramol. Chem.* **2011**, *23*, 304.
50. M. Hasegawa, H. Enozawa, Y. Kawabata, M. Iyoda, *J. Am. Chem. Soc.* **2007**, *129*, 3072.
51. *Electrochromic Materials and Devices.* R. J. Mortimer, D. R. Rosseinsky, P. M. Monk, Wiley-VCH, 2015.
52. S. Cong, Y. Tian, Q. Li, Z. Zhao, F. Geng, *Adv. Mater*. **2014**, *26*, 4260.
53. A. Patra, M. Bendikov, S. Chand, *Acc. Chem. Res.* **2014**, *47*, 1465.
54. G. Cai, J. Wang, P. S. Lee, *Acc. Chem. Res.* **2016**, *49*, 1469.
55. C. Reus, M. Stolar, J. Vanderkley, J. Nebauer, T. Baumgartner, *J. Am. Chem. Soc.* **2015**, *137*, 11710.
56. Q. Zhangm C.-Y. Tsai, L.-J. Li, D.-J. Liaw, *Nat. Commun.* **2019**, *10*, 1239.
57. D. P. Dubal, N. R. Chodankar, D.-H. Kim, P. Gomez-Romero, *Chem. Soc. Rev.*, **2018**, *47*, 2065.
58. Y. Alesanco, A. Viñuales, J. Rodriguez, R. Tena-Zaera, *Materials* **2018**, *11*, 414.
59. L. Shen, L. Du, S. Tan, Z. Zhang, C. Zhao, W. Mai, *Chem. Commun.* **2016**, *52*, 6296.
60. M. A. Invernale, Y. Ding, G. A. Sotzing, *Appl. Mater. Interfaces*, **2010**, *2*, 296.
61. M. Iyoda, M. Hasegawa, J. Takano, K. Hara, Y. Kuwatani, *Chem. Lett.* **2002**, *31*, 590.
62. K. Hara, M. Hasegawa, Y. Kuwatani, H. Enozawa, M. Iyoda, *Chem. Commun.* **2004**, 2042.
63. M. Hasegawa, Y. Kobayashi, K. Hara, H. Enozawa, M. Iyoda, *Heterocycles* **2009**, *77*, 837.
64. M. Iyoda, H. Enozawa, Y. Miyake, *Chem. Lett.* **2004**, 1098.
65. A. S. Anderson, K. Kilsa, T. Hassenkam, J. P. Gisselbrecht, C. Boudon, M. Gross, M. B. Nielsen, F. Diederich, *Chem. Eur. J.* **2006**, *12*, 8451.
66. K. Lincke, A. F. Frellsen, C. R. Parker, A. D. Bond, O. Hammerich, M. B. Nielsen, *Angew. Chem. Int. Ed*. **2012**, *51*, 6099.
67. H. Jiang, V. Mazzanti, C. R. Parker, S. L. Broman, J. H. Wallberg, K. Lušpai, A. Brincko, H. G. Kjaergaard, A. Kadziola, P. Rapta, O. Hammerich M. B. Nielsen, *Beilstein J. Org. Chem.* **2015**, *11*, 930.
68. M. Hasegawa, J. Takano, H. Enozawa, Y. Kuwatani, M. Iyoda, *Tetrahedron Lett*. **2004**, *45*, 4109.
69. Z. Chen, A. Lohr, C. R. Saha-Möller, F. Würthner, *Chem. Soc. Rev.* **2009**, *38*, 564.
70. Although two TTF moieties can locate close each other in **4a** and **4a**$^{\bullet+}$, there are no interactions through either S•••S or π-π contacts. This was supported by geometry optimization of **1c**$^{\bullet+}$ and its related compounds. See Figure S10.
71. M. Quinto, S. A. Jenekhe, A. J. Bard, *Chem. Mater.* **2001**, *13*, 2824.
72. L. Kong, M. Wang, X. Ju, J. Zhao, Y. Zhang, Y. Xie, *Polymer* **2017**, *9*, 656.
73. Color was gradually changed into initial purple after stopping of the voltage application.